A Self-Calibrating Mathematical Model for the Direct Piezoelectric Effect of a New MEMS Tilt Sensor

Paul M. Moubarak, *Student Member, IEEE*, Pinhas Ben-Tzvi, *Member, IEEE*, and Mona Elwakkad Zaghloul, *Fellow, IEEE*

***Abstract*—This paper presents a self-calibrating mathematical model and simulation results of the direct piezoelectric effect of a new tilt-sensor that measures inclination angles around two orthogonal axes. Using a fundamental description of the mechanical stress generated in suspended beams under static loading, we propose a model of the sensor's direct piezoelectric effect that is only a trigonometric function of its genetic behavior in two orthogonal planes. The significance of the proposed approach lies in the independence of the model from the structural dimensions of the piezo-system and the electro-mechanical properties of the piezoelectric layer. The effect of these structural properties and other external stimuli on the proposed model is implicitly contained, and inherently carried by the genetic data which is curve-fitted using a polynomial approximation. The feasibility of the proposed method and the accuracy of the model are verified by cross-comparison with simulation results. These simulations are performed on a CAD model of the piezoelectric tilt sensor for a *case-study* operation range of 0 – 90°. An overall considerable accuracy level was noted between the simulated and modeled data over the full operation range, with an average relative peak error of 1.9%.**

***Index Terms*—Direct piezoelectric effect, dual-axis inclination, mathematical modeling, self-calibration, tilt sensor.**

I. Introduction

THE direct piezoelectric effect that crystalline materials exhibit, either naturally or synthetically, is the byproduct of a complex electromechanical interface that affects the polarization of the crystal. This polarization, which defines the density of electric dipole moments in the crystal, induces an electric field across the surface of the solid. In the direct effect of piezoelectricity, the application of a mechanical stress on the faces of the crystal disturbs the stable orientation of the dipoles, forcing their respective realignment within the crystalline lattice. This dipole reconfiguration generates a change in the polarization which induces a proportional change in the electric field. From an applications perspective, the piezoelectric behavior of crystalline materials is of primary importance for the development of sensor technology, where the stress-inducing capability of a physical property, such as pressure [1] or acceleration [2], [3], is converted into a measurable metric, namely an electrical voltage.

Modeling the direct piezoelectric behavior of crystals has formally been done using constitutive equations, which relate the applied mechanical stress tensor T to the resulting electrical polarization D in the absence of an external electric field [4]. This electro-mechanical relationship is a function of the piezoelectric properties of the crystal, where the stress tensor T and the polarization vector D are correlated together through the piezoelectric coefficient matrix d. Likewise, the voltage V across the crystal's faces is related to the induced polarization D through the electrical permittivity ε. In this context, modeling the behavior of a piezoelectric system (sensor or actuator) using constitutive equations generates a mathematical representation that depends explicitly on the crystal properties d and ε. This representation also depends on the system's geometric dimensions and structural properties as exhibited in the stress tensor T.

This dependence of the constitutive equations on the system's geometrical, structural and piezoelectric properties renders the resulting mathematical model vulnerable to unpredictable, unstable or time-varying parameters. Coefficients d and ε – albeit well defined for commonly used piezoelectric materials such as Zinc Oxide (ZnO) and Lead Zirconate Titanate ($PbZrTiO_3$-$PbTiO_3$) – are inherently affected and subsequently altered by the operating conditions of the piezoelectric system. In the most common cases, the vulnerability of piezoelectric models can be attributed to one (or a combination) of the following conditions:

(a) *Temperature*: Large temperature fluctuations, such as during space (-165 – $195°C$) and underwater operations, generate a significant variation in matrix coefficients d [5]–[8] *and* ε [9] that drastically impacts the performance of the piezoelectric system. Temperature normally induces the biggest impact on the crystals' piezoelectric properties, but it equally affects the geometric characteristics of the micro-structure. Thermal expansion [10] generates thermal stress [11] and intrinsic structural deformations that affect the elements of the stress tensor T, specifically elements T_1, T_2 and T_3 that carry the bending moment components [12].

(b) *Fatigue and Aging*: Crystal characteristics can deteriorate under fatigue and aging effects due to the intrinsic process of spontaneous energy reduction. Fatigue behavior can be

Manuscript received July 18, 2011; revised September 29, 2011; accepted October 12, 2011. Date of publication October 21, 2011; date of current version April 06, 2012. The associate editor coordinating the review of this manuscript and approving it for publication was Prof. Gerald Gerlach.

P. M. Moubarak is with the Robotics and Mechatronics Laboratory, Department of Mechanical and Aerospace Engineering, and the School of Engineering and Applied Science, George Washington University, Washington, DC 20052 USA (e-mail: paul4@gwmail.gwu.edu).

P. Ben-Tzvi is with the School of Engineering and Applied Science and the Robotics and Mechatronics Lab, Department of Mechanical and Aerospace Engineering, George Washington University, Washington, DC 20052 USA (e-mail: bentzvi@gwu.edu).

M. E. Zaghloul is with the School of Engineering and Applied Science, the Department of Electrical Engineering, and the Department of Electrical and Computer Engineering, George Washington University, Washington, DC 20052 USA (e-mail: zaghloul@gwu.edu).

Color versions of one or more of the figures in this paper are available online at http://ieeexplore.ieee.org.

Digital Object Identifier 10.1109/JSEN.2011.2173188

induced thermally [13], electrically [14] (switching frequency) or mechanically [15] (recurring bending and deflections leading to disorientation of the domains), and results in aging deterioration that affects piezoelectric coefficients d [16] and permittivity ε [17].

(c) *Large Electric Fields*: Exposure to strong electric fields disturbs the alignment of the electric dipoles and degenerates the crystal characteristics. The deterioration of these characteristics is proportional to the strength of the field [18], and the latter can lead to complete depolarization of the piezoelectric material if the field strength exceeds a threshold limit. Strong electric fields are most commonly present in actuator applications that involve piezoelectric crystals and alternating AC signals [19], [20]. The depolarization effect of such sinusoidal signals is most significant during the half cycle that opposes the crystal's poling field.

Compensation for this performance degeneration is typically accomplished by characterizing the behavior of the crystal and its properties as a function of every external stimulus [21], [22] (temperature, cycles of operation, electric field, etc.). This approach generally adds more parameters to the mathematical representation and increases the complexity and non-linearity of the constitutive piezoelectric models.

However, for some piezoelectric applications such as biaxial tilt sensing; it is possible to eliminate model vulnerability to external stimuli by developing a self-calibrating mathematical representation of the direct piezoelectric effect through a fundamental derivation of the constitutive equations. By *self-calibration*, we mean that the resulting model will not explicitly depend on the system's piezoelectric or structural characteristics, nor will it depend on any external stimuli that may impact these characteristics. Rather, this information – which is present in the model in the form of curve-fitted data – will be implicitly carried by genetic data provided *a priori* about the operation of the piezo system.

Although such modeling methodology cannot *presently* be proven to being generalizable, its significance on system-to-system basis is highly desirable, especially for real-time applications where the system is subject to fabrication imperfections and recurrent variations in operating conditions. To concretize this significance, we propose in this paper a new piezoelectric tilt sensor that we employ as a case-study illustrative application. Genetic data from the operation of this tilt meter in two orthogonal planes is extracted and curve-fitted. Subsequently, a mathematical derivation that uses this data to generate a self-calibrating model of the sensor's general behavior is presented. The feasibility of the proposed method and the accuracy of the resulting model are verified by cross-comparison with simulation results performed over the sensor's full-range operation of 0–90°.

II. Dual-Axis MEMS Tilt Meter

A. Piezoelectric Tiltmeter: Concept of Operation

The piezoelectric tilt sensor introduced in this paper correlates the change in the static stress induced in suspended beams to the plane inclination (Fig. 1). Recently, physics such as optics [23], [24] and piezo-resistivity [25] have reportedly been studied for the development of multi-axes tilt sensors. In this paper, a thin layer of Lead Zirconate Titanate (PZT) deposited on the top surface of the beam where the peak stress occurs, converts the change in stress as a function of angular inclination to a measurable electrical voltage [26]. At this stage, it is important to note that the objective of this paper is not to exhaustively discuss the fabrication and to characterize the operation of the proposed tilt-sensor (such investigations will be reported subsequently). Rather, our aim is to present the sensor concept for piezoelectric biaxial tilt measurement, and extract genetic data about its operation in order to introduce thoroughly the proposed self-calibrating model of its direct piezoelectric effect.

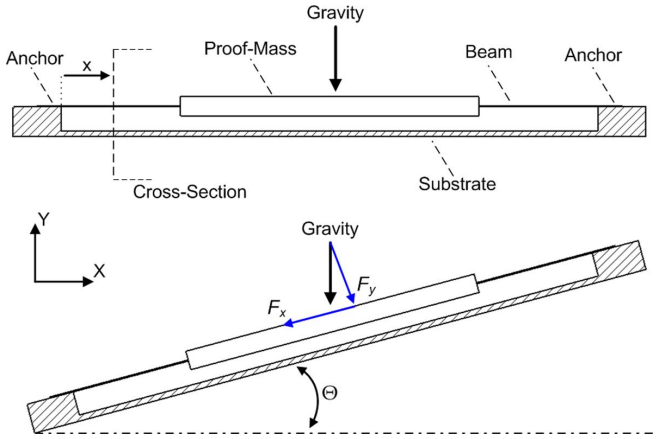

Fig. 1. Schematic representation of the tilt sensor in the horizontal and *single-axis* inclined position (Θ-rotation around the z-axis).

In this context, a schematic of the proposed tilt sensor is shown in Fig. 1. A substrate with a central cavity supports a thin beam anchored on both ends. The beam carries a proof mass in the center causing the beam to deform under gravitational loading. For the *single-axis* operation depicted in Fig. 1 (Θ-rotation around the z axis only), this static deformation induces three dimensional stress components along the beam. In particular, the main component, or the static stress (σ_x) along the beam's x-axis, can be expressed at any cross section in terms of the gravitational load as

$$\sigma_x = \frac{F_{axial}}{A} + \frac{M_z y}{I_z} \tag{1}$$

where F_{axial} is the load in the x-direction, A is the cross-sectional area of the beam, M_z is the bending moment around the z-axis, y is the coordinate of the beam's horizontal surface measured from the neutral fiber along the y axis and I_z is the area moment of inertia around the z-axis.

For an inclination of the beam defined by a rotation Θ around the z-axis, the axial load and the bending moment at a cross section of the beam located at a distance x from the left anchor (Fig. 1), vary as a function of Θ. These can be both expressed trigonometrically as

$$\begin{aligned} F_{axial} &= F_x = F\sin(\Theta) \\ M_z &= F_y d = F\cos(\Theta)x \end{aligned} \tag{2}$$

where $F = Mg$ represents the gravitational weight with M representing the combined mass of the beam and the proof-mass, and g the gravitational acceleration.

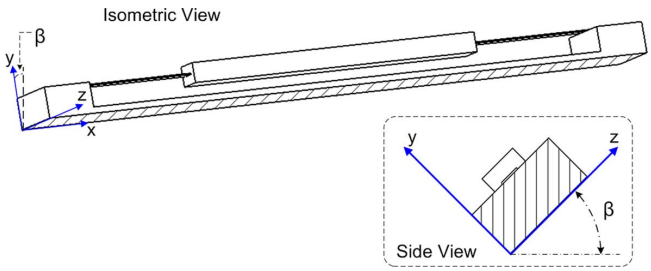

Fig. 2. Schematic representation of the tilt sensor in the single axis inclined position (β-rotation around the x-axis).

Thus, (1) can be re-written in terms of angle Θ as

$$\sigma_x(\Theta) = \frac{F\sin(\Theta)}{A} + \frac{F\cos(\Theta)x \cdot y}{I_z} \tag{3}$$

with a peak component σ_{peak} expressed in terms of Θ as

$$\sigma_{x_{peak}}(\Theta) = \frac{F\sin(\Theta)}{A} + \frac{F\cos(\Theta)x_{peak}y_{peak}}{I_z} \tag{4}$$

where x_{peak} and y_{peak} depict the location of the beam's cross section where the peak stress occurs. From the principles of strength of materials [27], y_{peak} corresponds to the top or bottom surface of the beam. Thus, a layer of PZT deposited on the top beam-surface where the peak stress occurs, generates a peak polarization D_{peak} that can be expressed in terms of the piezoelectric coefficient matrix d in the form of

$$D_{peak}\ (\Theta) = d \begin{bmatrix} \sigma_{x_{peak}}(\Theta) \\ T_2 \\ T_3 \\ T_4 \\ T_5 \\ T_6 \end{bmatrix} \tag{5}$$

where T_1 was substituted for $\sigma_{x\,peak}$.

Other tensor elements, such as T_4 for the single axis operation, can also be expressed in a similar scheme in terms of Θ using the components of gravitational weight F ($F_x(\Theta)$ and $F_y(\Theta)$). As such, (5) infers that the polarization vector D of the PZT layer is a direct function of the inclination angle Θ. This argument subsequently holds true for the peak electric field E_{peak}, and the resulting peak voltage V_{peak} across the faces of the PZT layer, which are also expressed as a function of Θ according to the equations

$$\begin{aligned} D_{peak}(\Theta) &= \varepsilon E_{peak}(\Theta) \\ V_{peak}(\Theta) &= \int_C E_{peak}(\Theta) \cdot dl \end{aligned} \tag{6}$$

with ε representing the permittivity of the piezo-layer.

Similarly, for the *single-axis* operation depicted in Fig. 2 (β-rotation around the x axis only), one can show using a similar derivation that the peak polarization and the resulting peak voltage are a function of β as described in the equation

$$\begin{aligned} D_{peak}(\beta) &= \varepsilon E_{peak}(\beta) \\ V_{peak}(\beta) &= \int_C E_{peak}(\beta) \cdot dl. \end{aligned} \tag{7}$$

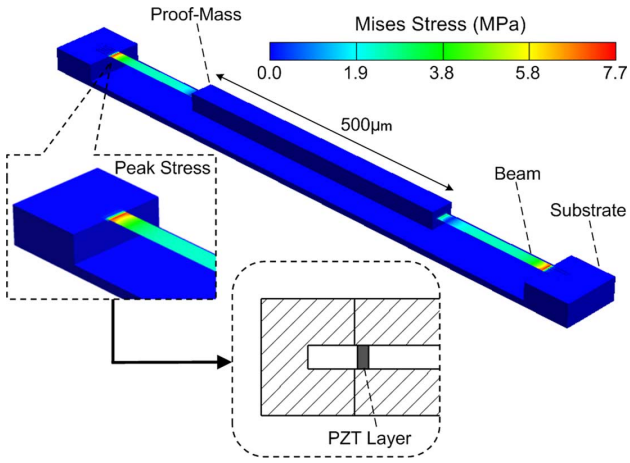

Fig. 3. FE stress profile of the sensor model in the horizontal position, with a schematic showing the PZT-layer deposited on the beam's top surface where the peak stress occurs.

B. Piezoelectric Tiltmeter: CAD Model and Single-Axis Simulation

A CAD model of the proposed tilt sensor was developed and simulated on *CoventorWare* software. The model consists of a silicon substrate with an etched central cavity that supports a fixed-fixed Platinum thin beam with a thickness of 0.2 μm. The proof mass, deposited in two stages symmetrically with respect to the beam, is also modeled with Platinum. This guarantees a heavy static load within a small volume, since the density of Platinum ($\rho = 21400\,\mathrm{Kg/m^3}$) is significantly higher than other MEMS metals such as Aluminum ($\rho = 2300\ \mathrm{Kg/m^3}$). The selected footprint of the proof mass is 500 μm$\times$ 40 μm, with a total thickness of 30.2 μm (including the thickness of the beam). The beam on the other hand has an active deflecting footprint of 900 μm$\times$ 20 μm (anchor to anchor) with a total tip-to-tip length of 980 μm (40 μm per anchor).

With this structure, the peak stress generated under static loading occurs when the sensor is in the horizontal position with $\Theta = 0°$ and $\beta = 0°$ as shown in Fig. 3. The peak stress value occurring near the anchors for the fixed-fixed beam is 7.2 MPa. This represents approximately 6% of the yield strength of Platinum. A PZT layer of 0.2 μm thickness and a footprint of 10 μm$\times$ 20 μm – deposited on the top surface of the beam where the peak stress occurs (Fig. 3) – converts the mechanical stress into a measurable voltage.

For a Θ-rotation of 0 – 90° around the z-axis, the change in the stress across the PZT layer according to (4) is shown in Fig. 4. The maximum Mises stress was plotted instead of individual stress components such as σ_x because CoventorWare does not generate individual parametric profiles for every stress component. In any case, the Mises stress and individual elements of the stress tensor all exhibit similar behaviors in terms of the inclination angle.

This change in the stress produces a proportional change in the PZT voltage, according to (6), which is shown in Fig. 5. The voltage range is 1896 – 0 μV for a Θ-inclination range of 0 – 90°, thus producing a sensitivity of 21 μV/Deg. It is worthwhile to note that the sensitivity of the sensor is a direct function of its geometry, and can be increased by modifying

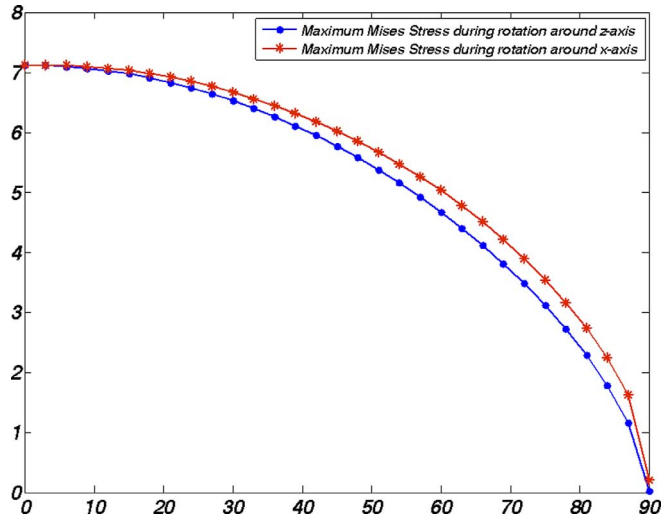

Fig. 4. Change in the peak Mises Stress across the beam as a function of the inclination angle (rotation around the z axis and rotation around the x-axis).

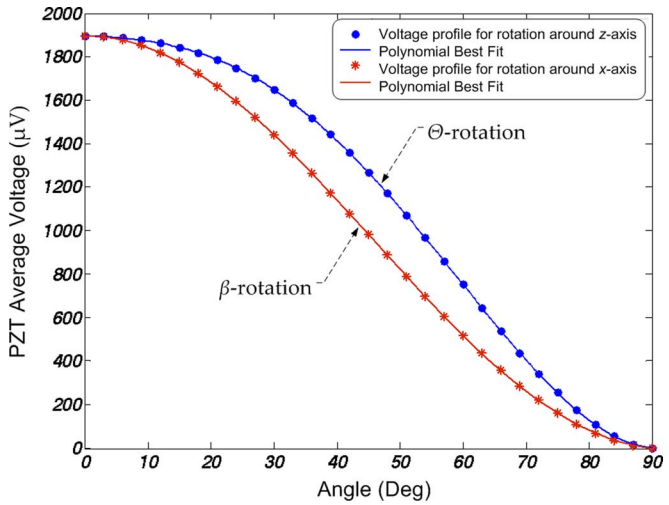

Fig. 5. Change in the average voltage across the PZT layer as a function of the inclination angle (Simulation data and corresponding polynomial best-fit).

its dimensions, such as increasing the length of the beam or increasing the weight of the proof mass.

On the other hand, a β-rotation of 0 – 90° around the x axis generates a different stress profile and a different corresponding voltage profile according to (7). These are shown respectively in Figs. 4 and 5. It should be noted that both voltage profiles (Θ-rotation & β-rotation) start from the same maximum value corresponding to the horizontal position of the sensor, and end at the same null value after a 90°-rotation around the z axis or the x-axis, respectively. The voltage profile in each case exhibits a unique interpolation between these two values with unique corresponding slope characteristics.

III. Self-Calibrating Model

The single axis behavior depicted in Fig. 5, whether during the x axis or the z axis rotation, can be accurately approximated by a fitted polynomial of low order. However, the more general dual axis operation of the sensor, where none of the two angles is held at zero, exhibits more complicated characteristics which cannot be approximated by a fitted curve. Rather, a more thorough derivation of the stress tensor and the constitutive equations is needed to mathematically characterize the full-range general behavior. Here, we propose to model the general dual axis response, which encompasses the more specific single axis behavior, by introducing a derivation that generates a self-calibrating model of the overall sensor behavior.

A. Hypothesis

The behavior of every piezoelectric system is inherently dictated by its structural and piezoelectric characteristics. Thus, if a specific genetic data about the operation of the piezo-system of Fig. 1 is given, and if this data can be curve-fitted, then a fundamental derivation of the constitutive equations will generate a system-specific mathematical model that describes the complete behavior of the piezo-system. The resulting model will represent a trigonometric function of the genetic data only. As such, the model will not depend explicitly on the system's structural and piezoelectric characteristics as this information is inherently carried by the genomic data.

Proof: Model Derivation

The genetic data of the piezoelectric tilt sensor is the single axis response shown in Fig. 5 for a β-rotation around the x axis and a Θ-rotation around the z-axis, respectively. For convenience, we define:

$V_{\beta,\Theta}$ as the PZT voltage-output for a random combination of angles β and Θ, $V_{\beta,0}$ as the PZT voltage-output for any angle β when $\Theta = 0°$, and $V_{0,\Theta}$ as the PZT voltage-output for any angle Θ when $\beta = 0°$.

Thus, using a 5th order polynomial approximation to curve-fit the genomic data of Fig. 5, we can express $V_{\beta,0}$ and $V_{0,\Theta}$ in terms of angles β and Θ , respectively, as follows

$$V_{\beta,0} = -2.88\times10^{-7}\beta^5 + 6.4\times10^{-5}\beta^4 + 3.43\times10^{-4}\beta^3 - 0.577\beta^2 + 0.349\beta + 1896 \quad (8)$$

$$V_{0,\Theta} = -1.08\times10^{-7}\Theta^5 + 10^{-4}\Theta^4 - 0.011\Theta^3 + 0.0256\Theta^2 - 1.97\Theta + 1899 \quad (9)$$

where $V_{\beta,0}$ and $V_{0,\Theta}$ are expressed in μV, and β and Θ (Deg) are measured with respect to the gravitational field which represents the reference direction.

Furthermore, a three-dimensional vector decomposition of the gravitational load F is considered, whose component magnitudes can be expressed (more conveniently) in the sensor's local frame xyz in terms of β and Θ as

$$\begin{aligned} F_x &= F\cos(\beta)\sin(\Theta) \\ F_y &= F\cos(\beta)\cos(\Theta) \\ F_z &= F\sin(\beta). \end{aligned} \quad (10)$$

From the piezoelectric characteristics of PZT [4], it is known that matrix d contains only five non-zero elements and can be written in the following general form

$$d = \begin{bmatrix} 0 & 0 & 0 & 0 & d_{15} & 0 \\ 0 & 0 & 0 & d_{24} & 0 & 0 \\ d_{31} & d_{32} & d_{33} & 0 & 0 & 0 \end{bmatrix}. \quad (11)$$

This means that component T_6 of the stress tensor does not contribute to the PZT voltage output. The remaining components can be expressed in terms of (10) as an explicit function of β and Θ, as follows

$$T_1 \triangleq \sigma_x = \frac{a_{11}F\cos(\beta)\sin(\Theta)}{A_x} + \frac{a_{12}F\cos(\beta)\cos(\Theta)x_p y_p}{I_z} + \frac{a_{13}F\sin(\beta)x_p z_p}{I_y} \tag{12}$$

$$T_2 \triangleq \sigma_y = \frac{a_{21}F\cos(\beta)\cos(\Theta)}{A_y} \tag{13}$$

$$T_3 \triangleq \sigma_z = \frac{a_{31}F\sin(\beta)}{A_z} \tag{14}$$

$$T_4 \triangleq \tau_{zy} = \frac{a_{41}F\cos(\beta)\cos(\Theta)Q_x}{I_x t_x} \tag{15}$$

$$T_5 \triangleq \tau_{xz} = \frac{a_{51}F\sin(\beta)Q_y}{I_y t_y} \tag{16}$$

where:

- A_x, A_y and A_z represent the area of the beam's cross section orthogonal to the x, y and z axes, respectively.
- I_x and I_y are the area moment of inertia of the beam's cross section around the x and y axes, respectively.
- Q_x and Q_y are the first moment of area of the beam's cross section around the x and y axes, respectively.
- t_x and t_y are the thickness of the cross section perpendicular to the corresponding shear and measured with respect to the beam's neutral fiber.
- x_p, y_p and z_p represent the coordinates of the points of interest on the beam where the calculation of the stress tensor is being performed.

Equations (15) and (16) of the shear stress are expressed according to *Jourawski* formula. In addition, coefficients $a_{ij} = cte$ of stress element T_i are added to the expression of the stress tensor for two reasons. First, a_{ij} accounts for the sign contribution of the corresponding term of element T_i, thus reflecting the tensile or compressive nature of individual terms. Second, a_{ij} aggregates all numerical constants relevant to every expression, such as the fraction of F that effectively contributes to the corresponding term of element T_i.

The components of the electric field can then be derived from the components of the stress vector and the permittivity ε according to the constitutive equations

$$\begin{aligned} D(\beta,\Theta) &= d\,T(\beta,\Theta) \\ E(\beta,\Theta) &= \varepsilon^{-1}D(\beta,\Theta). \end{aligned} \tag{17}$$

In the expanded expression of vector E in (17), we lump all coefficients and terms that are not an explicit function of angles β and Θ into coefficients k_i (which exhibit slight variations in terms of angles β and Θ). This simplifies the components of vector E to the following expressions

$$E_1 = k_1\sin(\beta) \tag{18}$$

$$E_2 = k_2\cos(\beta)\cos(\Theta) \tag{19}$$

$$E_3 = k_3\cos(\beta)\sin(\Theta) + k_4\cos(\beta)\cos(\Theta) + k_5\sin(\beta) + k_6\cos(\beta)\cos(\Theta) + k_7\sin(\beta). \tag{20}$$

Voltage $V_{\beta,\Theta}$ across the piezo-layer can then be calculated as a line integral of the dot product of the electrostatic field E and the infinitesimal vector displacement dl tangent to path C as

$$V_{\beta,\Theta} = \int_C E(\beta,\Theta)\cdot dl = E\cdot\hat{n}||\Delta L|| \tag{21}$$

where $\hat{n}$ denotes a unit vector in the ΔL direction, and $||\Delta L||$ denotes the magnitude of vector ΔL. The Cartesian components of vector ΔL and its subsequent magnitude, as well as the magnitude of vector E, can be written as follows

$$\begin{aligned} \Delta l &= (w+\delta w)\hat{x} + (t+\delta t)\hat{y} + (b+\delta b)\hat{z} \\ \Delta l &= ||\Delta l||\hat{n} = \sqrt{(w+\delta w)^2 + (t+\delta t)^2 + (b+\delta b)^2}\hat{n} \\ E &= ||E||\,\hat{e} \end{aligned} \tag{22}$$

where w, t and b denote the width, thickness and base length of the piezo-layer respectively, and δw, δt and δb denote the variation of each of these dimensions under tensile or compressive loading. $\hat{e}$ represents an arbitrary unit vector in the direction of the electric field E.

The dot product of (21) can be expanded in terms of the vector magnitudes as

$$V_{\beta,\Theta} = ||E||\;||\Delta L||\;\cos(\hat{e}\,,\hat{n}\,) = \lambda\,||E|| \tag{23}$$

with $\lambda = ||\Delta L||\cos(\hat{e},\hat{n})$ representing a geometric scalar that is an implicit function of angles β and Θ. The squared expression of (23) can be expanded as an explicit trigonometric function of angles β and Θ in the form of

$$\begin{aligned} V^2_{\beta,\Theta} &= K_1\sin^2(\beta) + K_2\cos^2(\beta)\cos^2(\Theta) \\ &\quad + K_3\cos^2(\beta)\sin^2(\Theta) + K_4\cos^2(\beta)\cos^2(\Theta) + K_5\sin^2(\beta) \\ &\quad + K_6\cos^2(\beta)\cos^2(\Theta) + K_7\sin^2(\beta) \\ &\quad + K_8\cos^2(\beta)\sin(\Theta)\cos(\Theta) + K_9\sin(\beta)\cos(\beta)\sin(\Theta) \\ &\quad + K_{10}\cos^2(\beta)\sin(\Theta)\cos(\Theta) + K_{11}\sin(\beta)\cos(\beta)\sin(\Theta) \\ &\quad + K_{12}\sin(\beta)\cos(\beta)\cos(\Theta) + K_{13}\cos^2(\beta)\cos^2(\Theta) \\ &\quad + K_{14}\sin(\beta)\cos(\beta)\cos(\Theta) + K_{15}\sin(\beta)\cos(\beta)\cos(\Theta) \\ &\quad + K_{16}\sin^2(\beta) + K_{17}\sin(\beta)\cos(\beta)\cos(\Theta) \end{aligned} \tag{24}$$

where coefficients

$$\begin{cases} K_{1-7} = \lambda^2\prod_{i=1}^{7} k_i k_i \\ K_{8-17} = 2\lambda^2\prod_{i=3}^{6}\prod_{j=i+1}^{7} k_i k_j \end{cases} \tag{25}$$

result from the expansion of the squared expressions of E_1, E_2 and E_3.

From (24), it becomes a simple task to derive trigonometric expressions for $V_{\beta,0}$ in (8) and $V_{0,\Theta}$ in (9) as a function of angles β and Θ, respectively. By setting $\Theta = 0°$ in (24), we get

$$\begin{aligned} V^2{}_{\beta,0} &= K_1\sin^2(\beta) + K_2\cos^2(\beta) + K_4\cos^2(\beta) \\ &\quad + K_5\sin^2(\beta) + K_6\cos^2(\beta) + K_7\sin^2(\beta) \\ &\quad + K_{12}\sin(\beta)\cos(\beta) + K_{13}\cos^2(\beta) \\ &\quad + K_{14}\sin(\beta)\cos(\beta) + K_{15}\sin(\beta)\cos(\beta) \\ &\quad + K_{16}\sin^2(\beta) + K_{17}\sin(\beta)\cos(\beta). \end{aligned} \tag{26}$$

Similarly, by setting $\beta = 0^\circ$ in (24), we get

$$\begin{aligned} &V^2_{0,\Theta} \\ &= K_2\cos^2(\Theta) + K_3\sin^2(\Theta) + K_4\cos^2(\Theta) \\ &\quad + K_6\cos^2(\Theta) + K_8\sin(\Theta)\cos(\Theta) + +K_{10}\sin(\Theta)\cos(\Theta) \\ &\quad + K_{13}\cos^2(\Theta). \end{aligned} \tag{27}$$

In (24), it is obvious that the terms with coefficients K_2, K_3, K_4, K_6, K_8, K_{10} and K_{13} can be replaced with $V^2_{0,\Theta}\cos^2(\beta)$. In the same context, the terms with the $\sin^2(\beta)$ in (24) (K_1, K_5, K_7 and K_{16}) can be substituted by an expression extracted from (27). After substitution, factorization and rearrangement of identical terms, (24) simplifies to

$$\begin{aligned} &V^2_{\beta,\Theta} \\ &= {V^2}_{0,\Theta}\cos^2(\beta) + {V^2}_{\beta,0} \\ &\quad - (K_2 + K_4 + K_6 + K_{13})\cos^2(\beta) \\ &\quad - (K_{12} + K_{14} + K_{15} + K_{17})\sin(\beta)\cos(\beta) \\ &\quad + (K_9 + K_{11})\cos(\beta)\sin(\beta)\sin(\Theta) \\ &\quad + (K_{12}+K_{14}+K_{15}+K_{17})\sin(\beta)\cos(\beta)\cos(\Theta). \end{aligned} \tag{28}$$

Equation (28) can be further simplified if one notices that $\beta = 0^\circ$ and $\Theta = 0^\circ$ in (24) yields

$$K_2 + K_4 + K_6 + K_{13} = {V^2}_{0,0}. \tag{29}$$

Thus, by defining parameters

$$\begin{aligned} m &= K_{12} + K_{14} + K_{15} + K_{17} \\ n &= K_9 + K_{11} \end{aligned} \tag{30}$$

we can reduce (28) to the final expression of

$$\begin{aligned} {V^2}_{\beta,\Theta} &= {V^2}_{0,\Theta}\cos^2(\beta) + {V^2}_{\beta,0} - {V^2}_{0,0}\cos^2(\beta) \\ &\quad + \sin(\beta)\cos(\beta)\ \{m\,(\cos(\Theta) - 1) + n\sin(\Theta)\} \end{aligned} \tag{31}$$

which represents the general expression of the voltage output of the piezo-layer as a function of the genomic data $V_{\beta,0}$ and $V_{0,\Theta}$ and inclination angles β and Θ. It is possible to further simplify (31) by defining

$$\boldsymbol{\mathcal{V}}_{\beta,\Theta} \triangleq V^2_{\beta,\Theta} \qquad \boldsymbol{\mathcal{V}}_{0,\Theta} \triangleq V^2_{0,\Theta} \qquad \boldsymbol{\mathcal{V}}_{\beta,0} \triangleq V^2_{\beta,0}$$

and rewriting (31) in its final expression of

$$\begin{aligned} \boldsymbol{\mathcal{V}}_{\beta,\Theta} &= \boldsymbol{\mathcal{V}}_{0,\Theta}\cos^2(\beta) + \boldsymbol{\mathcal{V}}_{\beta,0} - \boldsymbol{\mathcal{V}}_{0,0}\cos^2(\beta) \\ &\quad + \sin(\beta)\cos(\beta)\,\{m\,(\cos(\Theta) - 1) + n\sin(\Theta)\}. \end{aligned} \tag{32}$$

IV. Parameters Evaluation

The previous derivation showed that it is possible to model the general direct piezoelectric behavior of the case-study tilt-sensor as a trigonometric function of selected genetic data and inclination angles β and Θ. However, it also proved that the resulting expression (32) depends on two system-specific parameters m and n that need to be evaluated. These parameters encompass structural and piezoelectric properties of the beam and the PZT layer. Their evaluation can be accomplished by examining the boundary conditions and inspecting the first-derivative optimality condition of the tilt meter shown in Figs. 1 and 2.

A. Boundary Conditions

Using (32), one can inspect five different boundary conditions that are relevant to the *case-study* operation range of the sensor for angles β and Θ between $0 - 90^\circ$. These boundary conditions are listed as follows:

1) For $\beta = 0^\circ$ and $\Theta = 0^\circ$, the voltage output of the sensor should be $\boldsymbol{\mathcal{V}}_{0,0}$. Setting $\beta = \Theta = 0^\circ$ in (32) yields
$$\boldsymbol{\mathcal{V}}_{\beta,\Theta}|_{\beta=\Theta=0^\circ} = \boldsymbol{\mathcal{V}}_{0,0} \tag{33}$$
which verifies the first boundary condition.
2) For $\beta = 0^\circ\ \forall\theta$, the voltage profile of the sensor output should be identical to $\boldsymbol{\mathcal{V}}_{0,\Theta}$. Setting $\beta = 0^\circ$ in (32) yields
$$\boldsymbol{\mathcal{V}}_{\beta,\Theta}|_{\beta=0^\circ} = \boldsymbol{\mathcal{V}}_{0,\Theta} \tag{34}$$
which verifies the second boundary condition.
3) For $\Theta = 0^\circ\ \forall\beta$, the voltage profile of the sensor output should be identical to $\boldsymbol{\mathcal{V}}_{\beta,0}$. From (32), if we set $\Theta = 0^\circ$, we get
$$\boldsymbol{\mathcal{V}}_{\beta,\Theta}|_{\Theta=0^\circ} = \boldsymbol{\mathcal{V}}_{\beta,0} \tag{35}$$
which verifies the third boundary condition.
4) For $\beta = 90^\circ\ \forall\Theta$, the stress induced on the piezo layer is practically zero as reflected in Fig. 4. A zero-stress generates a negligible voltage output across the piezo layer faces. From (32), if we set $\beta = 90^\circ$, we get
$$\boldsymbol{\mathcal{V}}_{\beta,\Theta}|_{\beta=90^\circ} = \boldsymbol{\mathcal{V}}_{90^\circ,0} = 0 \tag{36}$$
which verifies the zero-voltage output of the PZT layer at 90°.
5) For $\Theta = 90^\circ\ \forall\beta$, the stress induced in the piezo layer is also near zero as reflected in Fig. 4. Setting $\Theta = 90^\circ$ in (32) yields the expression
$$\begin{aligned} \boldsymbol{\mathcal{V}}_{\beta,\Theta}|_{\Theta=90^\circ} &= \boldsymbol{\mathcal{V}}_{\beta,0} - \boldsymbol{\mathcal{V}}_{0,0}\cos^2(\beta) \\ &\quad + \sin(\beta)\cos(\beta)\{\,n - m\,\} = 0 \end{aligned} \tag{37}$$
in which $\boldsymbol{\mathcal{V}}_{0,90^\circ} = 0$ is immediately substituted based on the voltage profiles of Fig. 5. Equation (37) can be rearranged to yield the first equation for coefficients m and n, as follows
$$m - n = \frac{\boldsymbol{\mathcal{V}}_{\beta,0} - \boldsymbol{\mathcal{V}}_{0,0}\cos^2(\beta)}{\sin(\beta)\cos(\beta)}. \tag{38}$$

B. First Derivative Test

The exploration of the boundary conditions in the previous paragraph generated only one equation for the simultaneous

system of equations needed to derive unique expressions for coefficients m and n. To derive the required second equation, the first derivative of $\mathcal{V}_{\beta,\Theta}$ in (32) is inspected with respect to angle Θ. This derivative can be written as

$$\frac{\partial \mathcal{V}_{\beta,\Theta}}{\partial \Theta} = \mathcal{V}'_{0,\Theta}\cos^2(\beta) + \sin(\beta)\cos(\beta)\{-m\sin(\Theta) + n\cos(\Theta)\} \quad (39)$$

where $\mathcal{V}'_{0,\Theta}$ denotes the first derivative of $\mathcal{V}_{0,\Theta}$ with respect to Θ. Knowing that the voltage profile of the tilt meter peaks at $\Theta = 0^\circ\ \forall\beta$, the first optimality condition can be expressed using (39) as

$$\{\mathcal{V}'_{0,\Theta}\cos^2(\beta) + \sin(\beta)\cos(\beta)[-m\sin(\Theta) + n\cos(\Theta)]\}|_{\Theta=0^\circ} = 0 \quad (40)$$

which constitutes the second equation required to derive unique expressions for coefficients m and n. Using (38) and (40), these unique expressions are calculated as

$$m = \frac{-(\mathcal{V}'_{0,\Theta}|_{\Theta=0^\circ} + \mathcal{V}_{0,0})\cos^2(\beta) + \mathcal{V}_{\beta,0}}{\sin(\beta)\cos(\beta)}$$
$$n = -\mathcal{V}'_{0,\Theta}|_{\Theta=0^\circ}\cot an(\beta) \quad (41)$$

and accordingly, the equation of the voltage output $\mathcal{V}_{\beta,\Theta}$ in (32) can be updated – upon substitution of m and n – to the final expression of

$$\begin{aligned}\mathcal{V}_{\beta,\Theta} &= \mathcal{V}_{0,\Theta}\cos^2(\beta) + \mathcal{V}_{\beta,0} - \mathcal{V}_{0,0}\cos^2(\beta) \\ &+ (\cos(\Theta) - 1)\left\{\mathcal{V}_{\beta,0} - (\mathcal{V}'_{0,\Theta}|_{\Theta=0^\circ} + \mathcal{V}_{0,0})\cos^2(\beta)\right\} \\ &- \mathcal{V}'_{0,\Theta}|_{\Theta=0^\circ}\sin(\Theta)\cos^2(\beta). \quad (42)\end{aligned}$$

This concludes the proof of the hypothesis established in Section III-A, by deriving the final equation for the voltage profile $\mathcal{V}_{\beta,\Theta}$ of the tilt meter in terms of the genetic data $\mathcal{V}_{\beta,0}$, $\mathcal{V}_{0,\Theta}$ and the inclination angles β and Θ, only. The validity and performance accuracy of the self-calibrating direct piezoelectric model of (42) is subsequently verified through simulation results presented in the following section.

V. Simulation Results and Calibration Platform

A. Simulation Results

To validate the feasibility of the self-calibrating model presented in (42), the operation of the tilt meter of Fig. 3 was simulated on *ConventorWare* software for $0 \le \Theta \le 90^\circ$ and at sequential incremental values of β between 0 and 90°. Both the simulated and modeled profiles of the sensor output are plotted simultaneously in Figs. 6 – 8. As can be seen in these figures, the boundary conditions at $\Theta = 0^\circ$ and $\Theta = 90^\circ$ are well respected for all values of angle β, where every profile starts at the corresponding value of $\mathcal{V}_{\beta,0}$ and descends smoothly towards the zero output voltage at $\Theta = 90^\circ$.

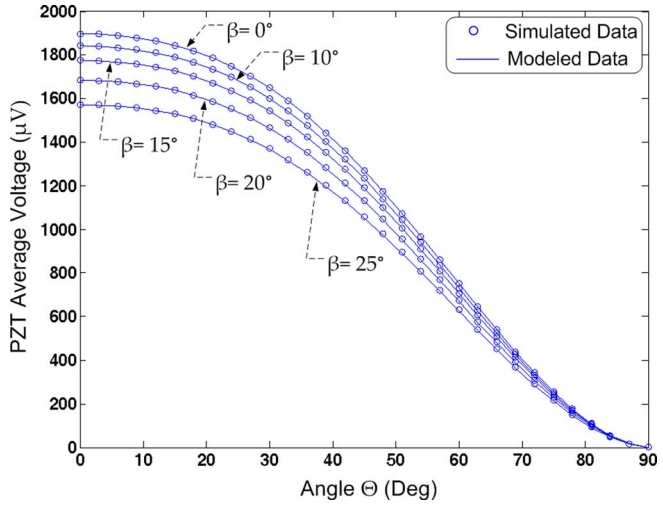

Fig. 6. Simulated data on *CoventorWare* (discrete blue points) and modeled data according to (42) (solid blue lines) for $0 \le \Theta \le 90^\circ$ and different values of angle β ($\beta = 0$, 10, 15, 20, 25°).

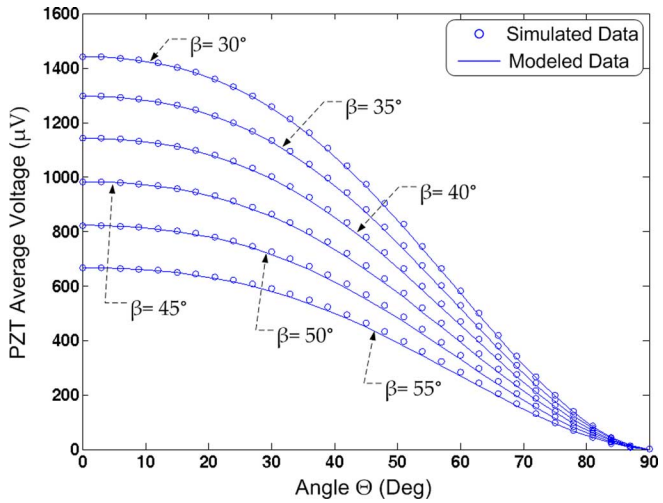

Fig. 7. Simulated data on *CoventorWare* (discrete blue points) and modeled data according to (42) (solid blue lines) for $0 \le \Theta \le 90^\circ$ and different values of angle β ($\beta = 30$, 35, 40, 45, 50. 55°).

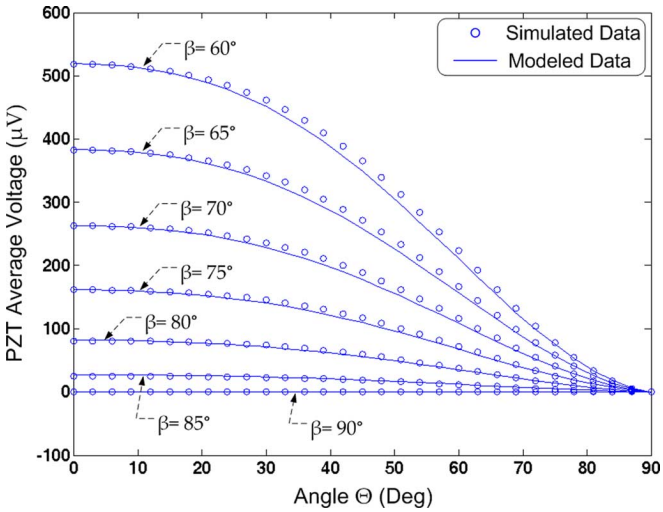

Fig. 8. Simulated data on *CoventorWare* (discrete blue points) and modeled data according to (42) (solid blue lines) for $0 \le \Theta \le 90^\circ$ and different values of angle β ($\beta = 60$, 65, 70, 75, 80. 85, 90°).

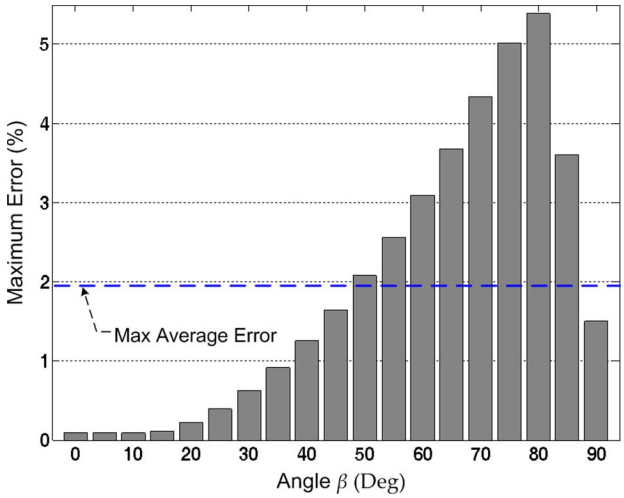

Fig. 9. A bar chart showing the maximum percent error (%) between the modeled data and the simulated data as a function of angle $0 \leq \beta \leq 90°$.

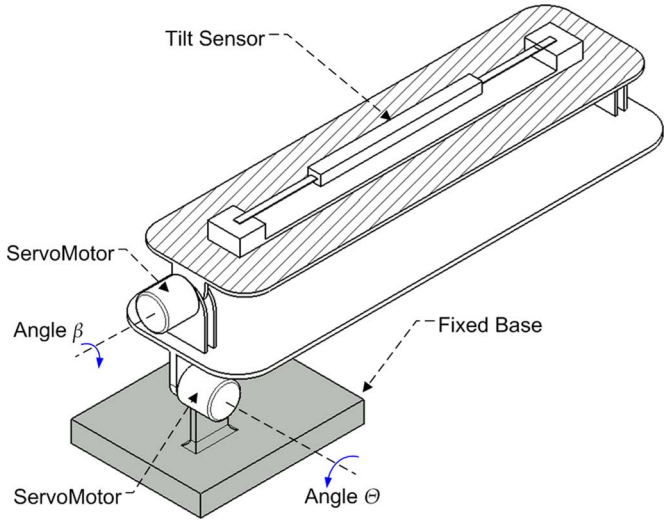

Fig. 10. Schematic of a candidate calibration platform with two servo-actuated joints (for angles β and Θ) to calibrate the tilt sensor and generate the genomic data $\boldsymbol{\mathcal{V}}_{\beta,0}$ and $\boldsymbol{\mathcal{V}}_{0,\Theta}$.

Although all profiles meet the boundary conditions $\forall\ \beta$, the error resulting from the voltage offset between the modeled data and the simulated data varies as a function of β and tends to increase with increasing β. This is most clearly reflected in Fig. 9 where the *maximum* percent error (%) between the modeled and simulated data is plotted in a bar chart as a function of angle β. With exception to the voltage profile at $\beta = 80°$, the maximum percent error in all other cases remains under 5%. Most notably, for $0 \leq \beta \leq 50°$ and at $\beta = 90°$, the maximum error is under 2%. The peak of the maximum percent errors occurs however at $\beta = 80°$, where the error reaches 5.37%. Such performance of the model is considerably acceptable, where overall, the model accuracy is characterized by an average maximum relative percent error of 1.9%.

B. Calibration Platform

In the previous discussions, we assumed that the genetic data about the operation of the tilt sensor was made available to the model described by (42). In reality, this data can be generated by calibrating the tilt sensor on a servo actuated platform with two joints. A candidate schematic of this platform is shown in Fig. 10. Each of the two joints of this platform corresponds to an angular variable relevant to the model described in (42). As such, to generate the genomic profile of $\boldsymbol{\mathcal{V}}_{\beta,0}$, the servo motor corresponding to angle β is actuated over the desired angular range (for instance, $0 \leq \beta \leq 90°$) while the motor corresponding to angle Θ remains at 0°. Readings from the piezo layer of the sensor are recorded at discrete intervals and the resulting profile is curve fitted to generate a polynomial expression for $\boldsymbol{\mathcal{V}}_{\beta,0}$ such as the one derived in (8).

In a similar scheme, a genomic profile for $\boldsymbol{\mathcal{V}}_{\beta,0}$ can be generated by actuating the servo motor corresponding to angle Θ over the desired angular range, while keeping the motor corresponding to angle β at 0°. Subsequent discrete recordings of the PZT output are curve-fitted to generate a polynomial expression for $\boldsymbol{\mathcal{V}}_{0,\Theta}$ similar to the one in (9).

The importance of this calibration method and the further relevance of the self-calibrating model of (42) is such that, if the platform is made small enough to be packaged with the sensor, this platform can be programmed to automatically recalibrate the sensor in order to update the genetic data and maintain the accuracy of the sensor. This capability can be most relevant for applications where the parameters that influence the electro-mechanical and piezoelectric properties of the sensor are expected to vary significantly as a function of the operating conditions (a good example would be space applications where the temperature fluctuates significantly over the course of one day).

VI. Conclusion

In this paper, we report the derivation and simulation results of a new self-calibrating model for the direct piezoelectric effect based on a proposed new design for a dual axis tilt sensor. The contribution of the model is such that it is completely independent of the electro-mechanical and piezoelectric characteristics of the sensor. The derived model relies solely on genetic data provided about the operation of the sensor in two orthogonal planes of the sensor's full range biaxial workspace. The accuracy and feasibility of the model was validated through simulation results, where the average maximum error resulting from the offset between the modeled data and the simulated data was $\sim 1.9\%$ for the full operation range ($0 \leq \beta \leq 90°$, $0 \leq \Theta \leq 90°$). Furthermore, this paper discussed a calibration platform that enables the generation of the genomic data. This platform possesses the ability to automatically recalibrate the sensor under fluctuations in the operating conditions in order to maintain the accuracy of the model.

In the future work, we would like to investigate the generalizable aspect of the proposed methodology of *self-calibrating piezoelectric modeling*. We also like to propose a method to further improve the accuracy of the sensor by adding an expression to the model in (42) derived from the null space of the boundary conditions. Our future investigations will equally address the inverse sensing problem with the experimental sensor, where angles β and Θ are numerically calculated from (42) for a given voltage output of the physical sensor. This will require

the derivation of a supplementary equation generated from an additional piezo layer deposited on an adjacent surface in order to guarantee the uniqueness of the inverse solution.

REFERENCES

[1] M. Akiyama, Y. Morofuji, T. Kamohara, K. Nishikubo, M. Tsubai, O. Fukuda, and N. Ueno, "Flexible piezoelectric pressure sensors using oriented aluminum nitride thin films prepared on polyethylene terephthalate films," *J. Appl. Phys.*, vol. 100, no. 11, pp. 114318–114318-5, Dec. 2006.

[2] Q. Zou, W. Tan, E. S. Kim, and G. E. Loeb, "Single- and triaxis piezoelectric-bimorph accelerometers," *J. Microelectromech. Syst.*, vol. 17, no. 1, pp. 45–57, Feb. 2008.

[3] L.-P. Wang, R. A. Wolf, Y. Wang, K. K. Deng, L. Zou, R. J. Davis, and S. Trolier-McKinstry, "Design, fabrication, and measurement of high-sensitivity piezoelectric microelectromechanical systems accelerometers," *J. Microelectromech. Syst.*, vol. 12, no. 4, pp. 433–439, Aug. 2003.

[4] C. Liu, *Foundations of MEMS*. Englewood Cliffs, NJ: Pearson Education, 2006, ch. 7.

[5] R. G. Sabata, B. K. Mukherjee, W. Ren, and G. Yang, "Temperature dependence of the complete material coefficients matrix of soft and hard doped piezoelectric lead zirconate titanate ceramics," *J. Appl. Phys.*, vol. 101, no. 6, pp. 064111–1–064111-7, Mar. 2007.

[6] B. Ivira, P. Benech, R. Fillit, F. Ndagijimana, P. Ancey, and G. Parat, "Modeling for temperature compensation and temperature characterizations of BAW resonators at GHz frequencies," *IEEE Trans. Ultrason., Ferroelectr., Frequency Control*, vol. 55, no. 2, pp. 421–430, Feb. 2008.

[7] R. A. Wolf and S. Trolier-McKinstrya, "Temperature dependence of the piezoelectric response in lead zirconate titanate films," *J. Appl. Phys.*, vol. 95, no. 3, pp. 1397–1397-10, Feb. 2004.

[8] G. Xu, X. Wang, D. Yang, Z. Duan, C. Feng, and K. Chen, "Peculiar temperature aging effects on the piezoelectric constant of $Pb(Mg_{1/3}Nb_{2/3})O_3$-$PbTiO_3$ single crystal near the morphotropic phase boundary," *Appl. Phys. Lett.*, vol. 86, no. 3, pp. 032902–1–032902-3, Jan. 2005.

[9] Z. Feng and X. Rena, "Aging effect and large recoverable electrostrain in Mn-doped $KNbO_3$-based ferroelectrics," *Appl. Phys. Lett.*, vol. 91, no. 3, pp. 032904–1–032904-3.

[10] G. Rogl, L. Zhang, P. Rogl, A. Grytsiv, M. Falmbigl, D. Rajs, M. Kriegisch, H. Müller, E. Bauer, J. Koppensteiner, W. Schranz, M. Zehetbauer, Z. Henkie, and M. B. Maple, "Thermal expansion of skutterudites," *J. Appl. Phys.*, vol. 107, no. 4, pp. 043507–1–043507-10, Feb. 2010.

[11] M. A. Moskqa, P. S. Ho, D. J. Mikalsen, J. J. Cuomo, and R. Rosenberg, "Measurement of thermal stress and stress relaxation in confined metal lines. I. Stresses during thermal cycling," *J. Appl. Phys.*, vol. 74, no. 3, pp. 1716–1716-9, Aug. 1993.

[12] M. Akiyama, K. Shobu, C.-N. Xu, K. Nonaka, and T. Watanabe, "Ceramic microtubes self-formed at room temperature that exhibit a large bending stress," *J. Appl. Phys.*, vol. 88, no. 7, pp. 4434–4434-3, Oct. 2000.

[13] C. K. Wonga, Y. M. Poon, and F. G. Shin, "Temperature dependence of the complex effective piezoelectric coefficient of ferroelectric 0–3 composites," *J. Appl. Phys.*, vol. 92, no. 6, pp. 3287–3287-6, Sep. 2002.

[14] K. Takemura, M. Ozgul, V. Bornand, S. Trolier-McKinstry, and C. Randallb, "Fatigue anisotropy in single crystal $Pb(Zn_{1/3}Nb_{2/3})O_3$-$PbTiO_3$," *J. Appl. Phys.*, vol. 88, no. 12, pp. 7272–7272-6, Dec. 2000.

[15] S. Pruvost, G. Sebald, L. Lebrun, and D. Guyomar, "Depolarization mechanism under compressive stress in $Pb(Mg_{1/3}Nb_{2/3})_{1-x}Ti_xO_3$," *J. Appl. Phys.*, vol. 102, no. 6, pp. 064104–064104-6, Sep. 2007.

[16] S. Priya, J. Ryu, K. Uchino, and D. Viehland, "Mechanical aging behavior of oriented $Pb(Mg_{1/3}Nb_{2/3})O_3$–$PbTiO_3$ and $Pb(Zn_{1/3}Nb_{2/3})O_3$–$PbTiO_3$ single crystals," *Appl. Phys. Lett.*, vol. 79, no. 16, pp. 2624–1–2624-3, Aug. 2001.

[17] H. Zhang, S. Jiang, J. Xiao, and K. Kajiyoshi, "Piezoelectric and dielectric aging of $Bi_{0.5}(Na_{0.82}K_{0.18})_{0.5}TiO_3$ lead-free ferroelectric thick films," *J. Appl. Phys.*, vol. 107, no. 12, pp. 124118–1–124118-6, Jun. 2010.

[18] V. D. Kugela and L. E. Cross, "Behavior of soft piezoelectric ceramics under high sinusoidal electric fields," *J. Appl. Phys.*, vol. 84, no. 5, pp. 2815–1–2815-16, Sep. 1998.

[19] W. Ren, S.-F. Liu, and B. K. Mukherjeea, "Nonlinear behavior of piezoelectric lead zinc niobate–lead titanate single crystals under AC electric fields and DC bias," *Appl. Phys. Lett.*, vol. 83, no. 25, pp. 5268–1–5268-3, Dec. 2003.

[20] H. Wang, A. A. Wereszczak, and H.-T. Lin, "Fatigue response of a PZT multilayer actuator under high-field electric cycling with mechanical preload," *J. Appl. Phys.*, vol. 105, no. 1, pp. 014112–1–014112-14, Jan. 2009.

[21] Q. Chen, T. Zhang, and Q.-M. Wang, "Frequency-temperature compensation of piezoelectric resonators by electric DC bias field," *IEEE Trans. Ultrason., Ferroelectr., Frequency Control*, vol. 52, no. 10, pp. 1627–1631, Oct. 2005.

[22] L. Quagliarella, N. Sasanelli, and V. Monaco, "Drift in posturography systems equipped with a piezoelectric force platform: Analysis and numerical compensation," *IEEE Trans. Instrum. Meas.*, vol. 57, no. 5, pp. 997–1004, May 2008.

[23] X. Dong, C. Zhan, K. Hu, P. Shum, and C. C. Chan, "Temperature-insensitive tilt sensor with strain-chirped fiber Bragg gratings," *IEEE Photon. Technol. Lett.*, vol. 17, no. 11, pp. 2394–2396, Nov. 2005.

[24] M. Norgia, I. Boniolo, M. Tanelli, S. M. Savaresi, and C. Svelto, "Optical sensors for real-time measurement of motorcycle tilt angle," *IEEE Trans. Instrum. Meas.*, vol. 58, no. 5, pp. 1640–1649, May 2009.

[25] L. Tang, K. Zhang, S. Chen, G. Zhang, and G. Liu, "MEMS inclinometer based on a novel piezoresistor structure," *J. Microelectron.*, vol. 40, no. 1, pp. 78–82, Jan. 2009.

[26] P. Moubarak and P. Ben-Tzvi, "Design and analysis of a new piezoelectric MEMS tilt sensor," in *Proc. IEEE Int. Symp. Robot. Environments*, Montreal, ON, Canada, 2011, pp. 83–88.

[27] N. Dowling, *Mechanical Behavior of Materials*. Englewood Cliffs, NJ: Prentice-Hall, 2007, ch. 13.

Paul M. Moubarak (S'10) received the M.S. degree in mechanical engineering from the University of Maryland, College Park, in 2007 with research focus on bioinstrumentation technology. He is currently working toward the Ph.D. degree at the Robotics and Mechatronics Lab, Department of Mechanical and Aerospace Engineering, George Washington University, Washington, DC. His M.S. thesis work involved the development of an autonomous gait analysis system that analyzes gait patterns in rodents for medical and pharmaceutical applications.

His main research interests include robotics and robotic applications, microscale technology, nonlinear systems, and convex optimization.

Pinhas Ben-Tzvi (M'08) received the B.Sc. degree (*summa cum laude*) from the Technion—Israel Institute of Technology, Haifa, Israel, in 2000, and the M.Sc. and Ph.D. degrees from the University of Toronto, Toronto, ON, Canada, in 2004 and 2008, respectively, both in mechanical engineering.

From 2000 to 2002, he was with General Electric Medical Systems, where he was an R&D Engineer working on the development and integration of medical diagnostic robotic and mechatronic systems (CT, PET, and PET/CT). He is currently an Assistant Professor with the Department of Mechanical and Aerospace Engineering and the Director of the Robotics and Mechatronics Laboratory, George Washington University, Washington, DC. His areas of research and academic interests are focused in robotics, mechatronics, intelligent autonomous systems, mobile robotic locomotion and manipulation, and smart materials-based development of novel sensors and actuators for biomedical and miniature mechatronic and microrobotic systems. He is an associate editor of the *International Journal of Control, Automation, and Systems*.

Dr. Ben-Tzvi is a member of the American Society of Mechanical Engineers (ASME).

Mona Elwakkad Zaghloul (F'96) received the B.S. degree in electrical engineering from Cairo University, Cairo, Egypt, in 1965, and the M.A.Sc. degree in electrical engineering, M.Math degree in applied analysis and computer science, and Ph.D. degree in electrical engineering from the University of Waterloo, Waterloo, ON, Canada, in 1970, 1971, and 1975, respectively.

She is currently a Professor and Chair of the Electrical and Computer Engineering Department, George Washington University, Washington, DC, where she is also Director of the Institute of MEMS and VLSI Technologies. She has published over 290 technical papers in the areas of circuits and systems, microelectronic system design, Microelctromechanical systems and Nanoelctromechanical systems (MEMS/NEMS). She also contributed to several books.

Dr. Zaghloul was the Vice President of the IEEE-Circuits and Systems Society Technical Activities (1999–2001). She received the 50th year Golden Jubilee Medal from the IEEE Circuits and Systems Society in recognition for outstanding contribution to the society. She was the IEEE Sensors Council President 2008–2009. She received Honorary Doctorate Degree of Engineering from University of Waterloo, Canada. She was awarded in 2010 The George Washington University School of Engineering and Applied Science Distinguished Researcher Award.